coatings

MDPI

Article

Preparation and Properties of Thick Tungsten Coating Electrodeposited from Na_2WO_4-WO_3-KCl-NaF Molten Salt System

Yusha Li [1,†], Xiaoxu Dong [1,†], Qing Liu [2], Yajie You [1], Zeyu Gao [1] and Yingchun Zhang [1,*]

[1] School of Materials Science and Engineering, University of Science and Technology Beijing, 30 Xueyuan Road, Haidian District, Beijing 100083, China; liyusha1011@163.com (Y.L.)
[2] State Key Laboratory of Advanced Metallurgy, University of Science and Technology Beijing, 30 Xueyuan Road, Haidian District, Beijing 100083, China
* Correspondence: zycustb@163.com
† These authors contributed equally to this work.

Abstract: The pulsed current electrodeposition method was employed for the first time to achieve tungsten coating with a thickness of 433.72 μm on a CuCrZr alloy from Na_2WO_4-WO_3-KCl-NaF molten salt. The microstructure of the coating was observed and the coating density, porosity, hardness, bonding strength, residual stress and oxygen content were tested. The results revealed that the tungsten coating exhibited desirable characteristics such as high density, absence of impurities, excellent adhesion to the matrix (53.16 MPa), residual compressive stress as surface stress, and good stability and durability. Moreover, this thick tungsten coating possesses high density and hardness, low oxygen content and porosity. This offers a novel solution to solve the challenging issue of the connection between tungsten material and heat sink material.

Keywords: tungsten coating; electrodeposition; molten salt; CuCrZr alloy

Citation: Li, Y.; Dong, X.; Liu, Q.; You, Y.; Gao, Z.; Zhang, Y. Preparation and Properties of Thick Tungsten Coating Electrodeposited from Na_2WO_4-WO_3-KCl-NaF Molten Salt System. *Coatings* **2024**, *14*, 1471. https://doi.org/10.3390/coatings14111471

Academic Editors: Tsvetanka Babeva, Gergana Alexieva and Rositsa Gergova

Received: 25 October 2024
Revised: 13 November 2024
Accepted: 14 November 2024
Published: 20 November 2024

1. Introduction

At present, the fusion energy is currently widely acknowledged as one of the most promising and ultimate sources of energy [1]. In order to optimize the utilization of fusion energy and ensure its continuous and stable release, experts have conducted extensive exploration and research, culminating in the proposal of the ITER plan, which aims to construct a controlled nuclear fusion reactor. The pursuit of controlled nuclear fusion has always been a pivotal challenge, with one of the most crucial aspects lying in the development of the plasma-oriented material [2,3]. The progress and implementation of the ITER project are anticipated to yield a breakthrough in controllable nuclear fusion technology while offering an effective mitigation strategy for the global energy crisis.

The manufacturing technology of the cladding system is also a key requirement for the construction of the ITER project. The first wall material is significantly affected by high-energy neutrons, electromagnetic radiation and high-energy particles (such as atmospheric gases, nitrogen, helium and impurities) emitted from the plasma, which consists of plasma-oriented material, intermediate heat sink material and supporting backplane material and serves as the core component of the cladding system. Currently, the CuZrCr alloy is used as the heat sink material. And tungsten's exceptional properties such as its high melting point, excellent thermal conductivity, impressive strength, low coefficient of thermal expansion, negligible vapor pressure, minimal tritium-retention capability, low sputtering yield and high sputtering threshold have made it a primary choice for plasma materials [4,5]. However, tungsten and copper exhibit significant differences in physical properties primarily attributed to their large difference in thermal expansion coefficients. This discrepancy poses challenges in combining these two materials effectively and consequently limits the application of tungsten in plasma surface materials [6,7]. Therefore, alternative approaches such as coating or other viable connection technologies

are being considered. These methods involve applying a layer of tungsten coating onto a matrix material to serve as both a plasma-facing material and structural component [8,9]. Therefore, alternative approaches such as coating or other viable connection technologies are being considered. These methods involve applying a layer of tungsten coating onto a matrix material to serve as both a plasma-facing material and a structural component.

Currently, plasma spraying (PS), chemical vapor deposition (CVD), physical vapor deposition (PVD) and other coating technologies have been extensively employed for the preparation of tungsten coatings. The PS technique is known for its operational simplicity; nevertheless, it frequently yields tungsten coatings with intrinsic flaws like porosity or cracks [10]. The CVD method provides a rapid deposition rate for tungsten coatings, albeit requiring elevated temperatures [11]. Tungsten coatings via the PVD method demonstrate exceptional quality; nonetheless, depositing thick coatings utilizing this approach presents challenges and entails substantial expenses [12]. The molten salt electrodeposition (MSE) technique is emerging as a promising approach for the fabrication of metal coatings due to its cost-effectiveness and straightforward operational procedure. The coating prepared via MSE exhibits a strong adhesion to the substrate, high compactness, low porosity and tunable crystalline structure [13]. The molten salts utilized for tungsten electroplating encompass oxide and haloide-oxide compositions. The tungsten coating deposition in the oxide system does not require harsh external environmental conditions, and the preparation, purification, storage and transportation of molten salt are relatively straightforward, rendering it a flexible and practical choice for practical applications. Ningbo Sun and Fan Jiang et al. [14,15] electrodeposited tungsten coatings in Na_2WO_4-WO_3 molten salt at 1173 K. Wenxuan Qin et al. explored the reduction mechanism of tungsten ion at 1173 K by incorporating CeO_2, ZrO_2, La_2O_3 and Y_2O_3 into the Na_2WO_4-WO_3 molten salt system and subsequently achieved electrodeposition to obtain tungsten coatings with varying qualities [16]. However, due to the generally high melting point of pure oxide molten salts, it is necessary to increase the electrodeposition temperature. High temperatures will limit the choice of substrates and experimental equipment. In order to lower the electrodeposition temperature of tungsten coating, researchers have started utilizing halide molten salt systems, such as LiF-KCl-Li_2WO_4 [17], KF-KCl-WO_3 [18], NaCl-KCl-NF-WO_3 [19] and other molten salts. The addition of a certain amount of halide to the oxide has indeed proven effective in reducing the electrodeposition temperature.

The aim of this study is to establish a robust bonding between tungsten coating and CuCrZr alloy from the Na_2WO_4-WO_3-KCl-NaF low-temperature molten salt system using the molten salt electrodeposition method, while simultaneously increasing the thickness of the tungsten coating by extending the duration of electrodeposition. This research will offer a novel solution to solve the challenging issue of the connection between tungsten material and heat sink material, while establishing a strong foundation for their further optimization and practical application promotion.

2. Experiment and Parameters

2.1. Coating Deposition

The electrodeposition of tungsten coating from the Na_2WO_4-WO_3 molten salt system using the molten salt electrodeposition method was investigated by our group. Moreover, the incorporation of chloride ions can reduce the required temperature for electrodeposition. The Na_2WO_4-WO_3-KCl-NaF molten salt system was employed in this study to reduce the deposition temperature, and experiments were conducted based on the previously established electrodeposition parameters. $Na_2WO_4{\cdot}2H_2O$ (purity: 99.5%), WO_3 (purity: 99.5%), KCl (purity: 99.5%) and NaF (purity: 99.5%) in molten salt were all analytically pure. $Na_2WO_4{\cdot}2H_2O$ was dried for 24 h at 400 °C in order to remove the crystal water; WO_3, KCl and NaF were dried for 10 h at 200 °C. The dried Na_2WO_4, WO_3, KCl and NaF were mixed into an alumina crucible at 3:1:1:1 mol% proportion and then put into an electric furnace. The substrate was CuCrZr alloy, which served as the anode electrode. A tungsten plate (purity: 99.99%) was used as the cathode electrode. The specific elements

and contents of CuCrZr alloys are given in Table 1. Prior to electrodeposition, the electrodes were mechanically polished to obtain smooth surfaces and then ultrasonically cleaned in distilled water and alcohol solutions to obtain clean surfaces. The temperature of the electric furnace increases at a rate of 5 °C/min, reaching the electrodeposition temperature. The current density was set from 30 mA/cm^2, which is the average current. The frequency and duty cycle were set as 1000 Hz and 30%, respectively. After electrodeposition, the samples were put in NaOH solution for ultrasonic washing to eliminate the adherent salts.

Table 1. Elements and contents of CuCrZr alloy (wt.%).

Cu	Cr	Zr	Impurities
base	0.653	0.132	<0.075

2.2. Coating Characterization

The surface and cross-sectional morphology of the coated samples were observed by scanning electron microscopy (SEM, JSM6480LV, JEOL, Tokyo, Japan) with elemental analysis. The phase and crystal orientation of W coatings were detected by X-ray diffraction (XRD, Rigaku Industrial Co., Ltd., Tokyo, Japan, D/MAX-BB). The bonding strength was measured by tensile means using a universal testing machine. The tungsten-coating sample was attached to the mating plate with binders and the tensile rate was set to 1 mm/min until the sample fractured. The relative density was measured by the Archimedes method. The porosity of tungsten coatings was tested using a mercury injection apparatus (PM33GT-17, Quantachrome, Boynton Beach, FL, USA). The microhardness of the coating surface was measured using an MH-6 microhardness tester. The residual stress on the surface of the tungsten coating was determined through X-ray diffraction in this study. By measuring the corresponding 2θ angle at different values of ψ, and subsequently applying the least square method, we obtained the slope M from the 2θ-sin2ψ (X-Y) curve. The thermal conductivity of the tungsten coating was measured using the LFA 467HT laser thermal conductivity meter manufactured by NETZSCH in Selb, Germany.

3. Results and Discussions

3.1. Microstructure and Crystal Structure of Thick Tungsten Coating

The suitable temperature conditions for preparing tungsten coating in the Na_2WO_4-WO_3-KCl-NaF molten salt system were investigated in previous experiments. Through multiple experimental groups and test analyses, it was determined that an electrodeposition temperature of 780 °C yielded an ideal surface quality for electrodeposition tungsten coating. Electrodepositing thick tungsten coatings with high thermal conductivity poses a significant challenge as the coating thickness directly impacts its corrosion resistance against ionic radiation. Therefore, this paper aims to prepare thick tungsten coatings by extending the electrodeposition time. Additionally, the microstructure and properties of these thick tungsten coatings will be studied to observe their growth mechanism and performance characteristics. Table 2 provides the details on the electrodeposition parameters.

Table 2. Electrochemical parameters of electrodeposition thick tungsten coating.

Deposition Time (h)	Temperature (°C)	Current Density (mA/cm^2)	Duty Cycle (%)	Frequency (Hz)
50 100	780	30	30	1000

The surface morphology of tungsten coating, depicted in Figure 1, was achieved through electrodeposition times of 50 h and 100 h. It is evident that a layer of silver-gray coating is uniformly deposited on the CuCrZr matrix, exhibiting excellent coverage without any apparent cracks or holes. However, with the increase in electrodeposition time, the macroscopic morphology of the coating changes obviously. After 50 h electrodeposition,

the overall surface of the tungsten coating is uniform and dense, and large particles begin to appear. With an extension to a deposition time of 100 h, there is a significant increase in coating thickness due to continuous growth and accumulation on the substrate during a prolonged electrodeposition process. Nevertheless, locally present visible particles contribute to a rougher surface texture primarily attributed to changes in diffusion and migration rates of tungsten ions during extended deposition processes, leading to increased non-uniformity in crystal growth.

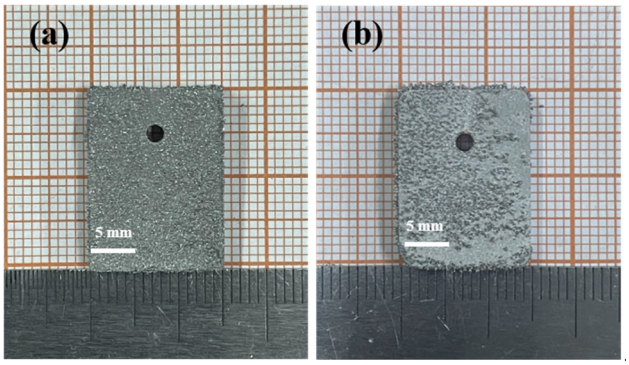

Figure 1. Macroscopic morphology of tungsten coatings at different deposition times: (**a**) 50 h, (**b**) 100 h.

The SEM image in Figure 2 depicts the highly compacted surface of the thick tungsten coating, exhibiting a lack of discernible gaps or cracks, which is consistent with the macroscopic morphology. When the electrodeposition time is 50 h, the grain size on the surface of the coating is large, but the arrangement is dense and the distribution is uniform. Upon reaching an electrodeposition time of 100 h, densification remains satisfactory but there is a notable increase in grain size accompanied by non-uniform distribution. This can be attributed to an extended deposition process that further retards the tungsten deposition rate while promoting grain growth and resulting in larger grain sizes and localized aggregation.

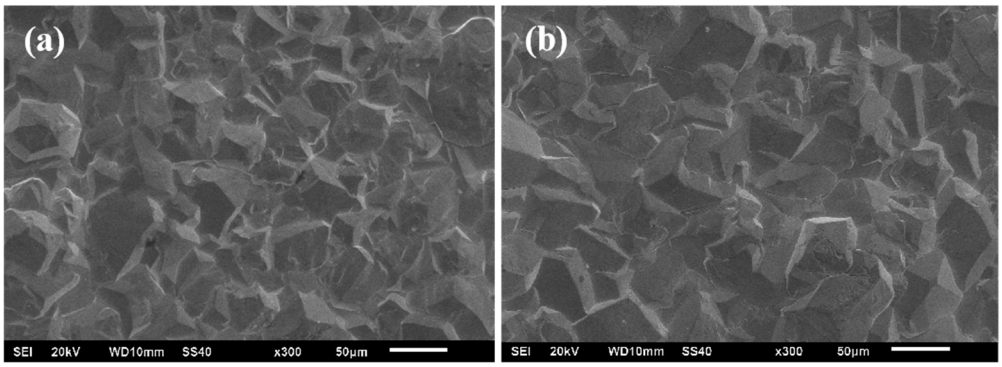

Figure 2. Surface SEM images of the tungsten coatings at different deposition times: (**a**) 50 h, (**b**) 100 h.

The surface roughness of the tungsten coating was analyzed using the laser confocal microscope. Image magnification of 200 times was selected to capture intricate details of the coating's surface topography, resulting in obtaining the laser confocal image shown in Figure 3. The experimental findings indicate that extending the electrodeposition time from 50 h to 100 h significantly increases the Ra value of the metal tungsten coating's surface roughness, from 7.469 μm to 10.322 μm. This indicates that with the increase in electrodeposition time, particles accumulate and grow on the surface of the coating, resulting in uneven particle distribution. Consequently, this non-uniformity results in an increase in surface roughness for the coating. However, it should be noted that while increasing electrodeposition time leads to higher surface roughness for thick coatings, such changes are not necessarily unfavorable in practical applications. In fact, under certain circumstances, deliberately increasing the roughness of coatings may enhance

the bonding force with substrates or improve other specific properties. Therefore, when optimizing electrodeposition processes, striking the balance between achieving desired levels of surface roughness for coatings while considering other relevant properties based on specific application requirements becomes crucial.

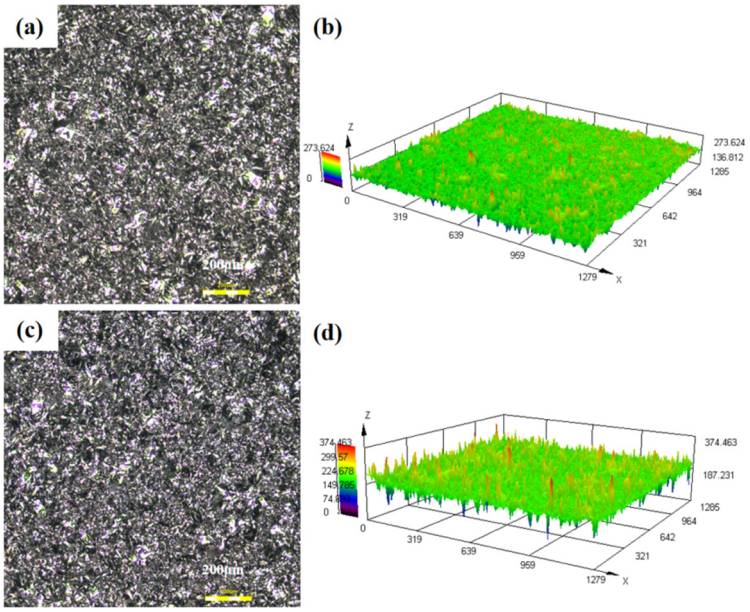

Figure 3. Laser confocal image of tungsten coating surface: (**a**) 50 h, 2D, (**b**) 50 h, 3D, (**c**) 100 h, 2D, (**d**) 100 h, 3D.

The X-ray diffraction (XRD) patterns of the thick tungsten coatings at different electrodeposition times are presented in Figure 4. As shown, the tungsten coating obtained after 50 h and 100 h of electrodeposition exhibits four distinct diffraction peaks located at 2θ values of 40°, 58°, 73° and 87°, respectively. These angles correspond to the crystallographic planes (110), (200), (211) and (220) of tungsten according to the standard XRD cards for tungsten. This confirms that the tungsten coating possesses exceptional crystallinity without any presence of impurity phases. Notably, both the (110) and (211) crystallographic planes exhibit relatively high diffraction peak intensities, indicating their dominance in the structure of the tungsten coatings.

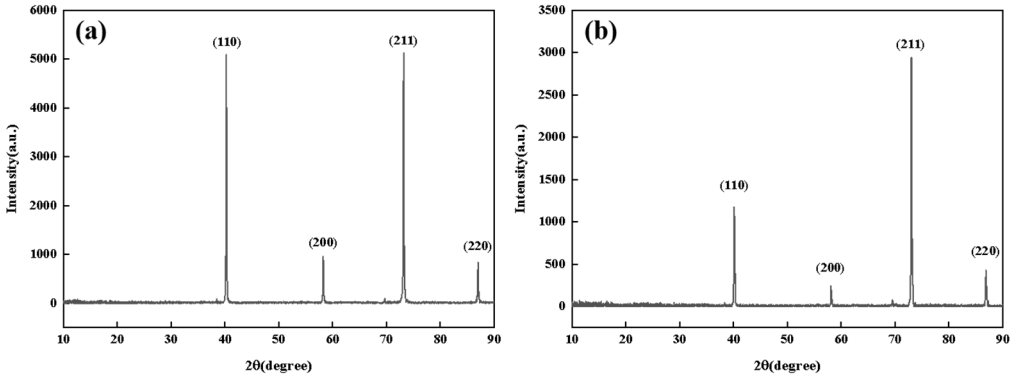

Figure 4. XRD patterns of tungsten coatings at different deposition times: (**a**) 50 h, (**b**) 100 h.

After comparing the XRD patterns of the tungsten coating with different electrodeposition times, it can be observed that the diffraction peak intensity of the (211) crystal plane relative to the (110) crystal plane is enhanced following a 100 h electrodeposition period. This enhancement suggests that during prolonged electrodeposition, the grains in the coating exhibit accelerated growth along the direction of the (211) crystal plane,

resulting in a corresponding increase in diffraction peak intensity for this particular crystal plane. Simultaneously, these findings also indicate how electrodeposition conditions influence the crystal structure of the coating by promoting a larger proportion or more orderly arrangement of (211) crystal faces within the coatings.

The electrodeposition time exerts a significant influence on the thickness of the tungsten coating during molten salt electrodeposition preparation. The SEM diagram depicted in Figure 5 reveals the section morphology and variations in coating thickness under different deposition times. After 50 h and 100 h electrodeposition, the strong bond between the tungsten coatings and the substrate are observed without any separation phenomenon. Specifically, with a deposition time of 50 h, the coating maintains an elevated level with a thickness measuring 310.65 μm, whereas with a deposition time of 100 h, it forms a thicker tungsten coating reaching up to 433.72 μm.

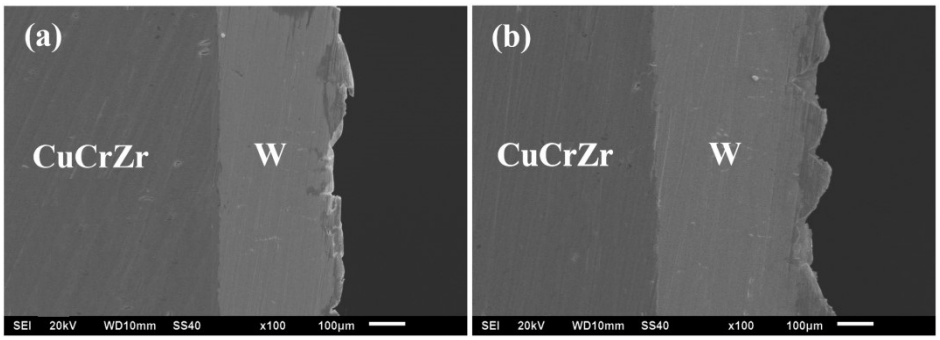

Figure 5. Cross-sectional SEM images of tungsten coatings at different deposition times: (**a**) 50 h, (**b**) 100 h.

The sectional line scanning of the coating electrodeposited after 100 h is illustrated in Figure 6. It can be observed from the line scanning that a negligible diffusion layer is evident, while the coating exhibits a robust adhesion to the matrix without any discernible voids or fractures.

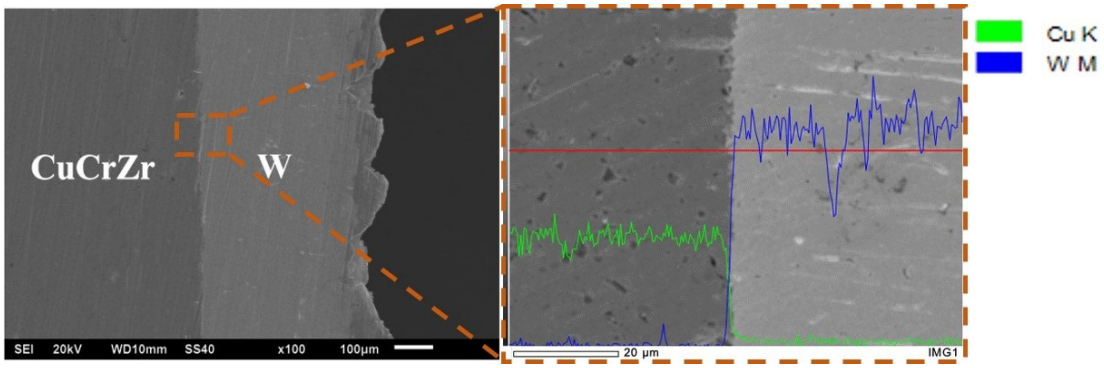

Figure 6. The sectional line scanning of the coating obtained after 100 h.

3.2. The Performance Evaluation of Thick Tungsten Coatings

The main physical properties of 50 h and 100 h electrodeposited tungsten coatings are presented in Table 3. Upon comparing the two datasets, it can be observed that the density of the coating increased from 18.71 g/cm^3 to 18.73 g/cm^3 as the electrodeposition time was extended from 50 h to 100 h. This indicates that with prolonged electrodeposition time, there is an enhancement in coating quality accompanied by a corresponding increase in density due to greater deposition of tungsten on the substrate, resulting in a thicker and denser coating layer. Furthermore, as the electrodeposition time increased, there was a decrease in coating porosity from 1.18% to 1.16%, along with a reduction in oxygen content from 0.032 wt.% to 0.028 wt.%. These changes can be attributed to long electrodeposition durations leading to densification of the coating and reduced porosity, thereby minimizing

opportunities for oxygen interaction with tungsten metal within the coating structure. However, overall variations were relatively minor, indicating that properties obtained through long-duration electrodeposition remain stable.

Table 3. Physical properties of thick tungsten coatings.

Deposition Time (h)	Density (g/cm^3)	Porosity (%)	Oxygen Content (%)
50	18.71	1.18	0.032
100	18.73	1.16	0.028

The hardness values of the coatings obtained by electrodeposition for 50 h and 100 h are presented in Table 4. The experimental findings demonstrate that long-term electrodeposition results in relatively high coating hardness due to enhanced arrangement of tungsten particles, optimized grain structure and improved mechanical properties. At the deposition time of 50 h, the microhardness of the coating is approximately 562.37 HV, which further increases to 568.84 HV when the deposition time is extended to 100 h. The increase in deposition time enables the full growth and development of tungsten crystals within the coating, resulting in the formation of stable structures. In this experiment, the tensile method was employed to assess the adhesive strength between the thick coating and the substrate. The test results are presented in Table 4. The experimental data demonstrate that after 50 h and 100 h electrodeposition, the bonding strength between the coatings and substrate is approximately 50 MPa. Moreover, with an electrodeposition time of 100 h, the bonding strength increases to reach 53.16 MPa. Deposition time facilitates more comprehensive interfacial reactions between the coating and substrate, resulting in improved growth and arrangement of coating grains as well as reduced defects and voids. As a result, the density of the coating is enhanced, as is the interface binding force between the coating and the substrate.

Table 4. Mechanical properties of thick tungsten coatings.

Deposition Time (h)	Hardness (HV)	Bonding Strength (MPa)
50	562.37	49.28
100	568.84	53.16

The residual stress in the coating plays a crucial role in determining the quality and performance. The residual stress intensifies the phenomenon of stress concentration inside the material, which makes the coating easy to crack at the interface. This also promotes the formation and expansion of micro-cracks, ultimately impacting the service life and reliability of the coating. On the other hand, residual compressive stress helps alleviate stress concentration within the material, enhancing its fatigue performance and resistance to external stresses. Consequently, it extends the overall service life of the coating. To measure this surface residual stress on the coating, an X-ray diffraction method was employed in this experiment. Table 5 presents peak 2θ values for tungsten coatings during an electrodeposition time of 50 h along with their corresponding $\sin^2(\Psi)$ values. Figure 7 illustrates a linear fitting analysis with a slope value of 0.245. The resulting residual stress is −309 MPa (negative), indicating that there exists residual compressive stress within the coating. The thick tungsten coating exhibits significant surface residual compressive stress due to volume-shrinkage inconsistencies caused by rapid cooling from high-temperature molten salt conditions. Thermal stresses primarily contribute to these differences, with thicker coatings experiencing greater disparities in cooling times, leading to increased surface residual compressive stresses.

Table 5. The peak value and $\sin^2(\Psi)$ of tungsten coating after 50 h electrodeposition.

$\sin^2(\Psi)$	0	0.1	0.2	0.3	0.4	0.5	0.6
2θ	131.188	131.209	131.237	131.253	131.289	131.310	131.332

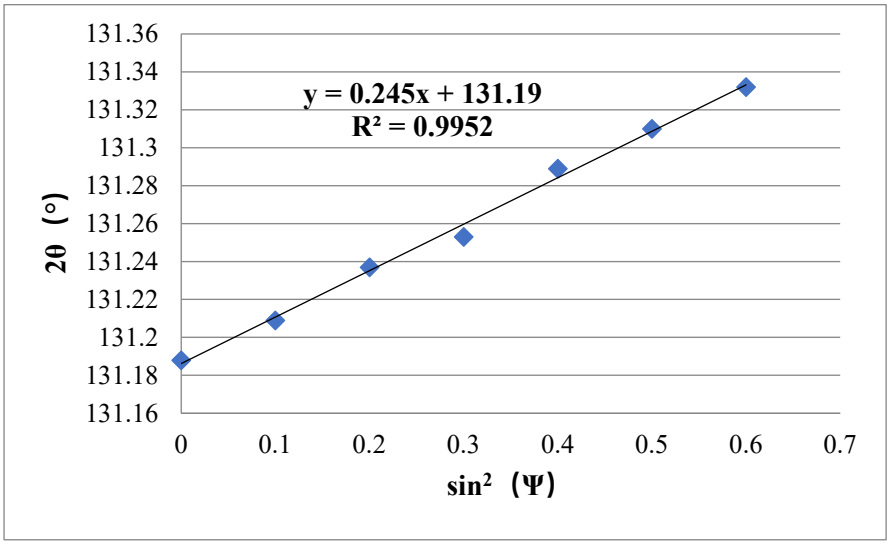

Figure 7. Linear fitting curve of peak 2θ and $\sin^2(\Psi)$.

4. Conclusions

In this paper, thick tungsten coating was obtained from Na_2WO_4-WO_3-KCl-NaF molten salt on the surface of a CuCrZr alloy at 780 °C, 30 mA/cm^2 current density, 30% duty cycle and 1000 Hz frequency. The microstructure and crystal structure of a thick tungsten coating were studied. The hardness, bonding strength, oxygen content, residual stress and thermal conductivity of the thick tungsten coating were measured.

A tungsten coating on a CuCrZr alloy surface can be successfully obtained from Na_2WO_4-WO_3-KCl-NaF low-temperature molten salt by the electrodeposition method. The electrodeposition time is extended to 100 h, and the thickness of the tungsten coating is increased to 433.72 μm. The adhesion strength between the thick tungsten coating and the CuCrZr alloy surface is good, measuring 53.16 MPa, while the hardness value reaches 568.84 HV. Moreover, the thick tungsten coating demonstrates high density, low oxygen content and minimal porosity. The residual stress calculations indicate that the deposited coating experiences residual compressive stress due to inconsistent volume shrinkage resulting from rapid cooling under high-temperature molten salt conditions.

Author Contributions: Formal analysis, Z.G.; Investigation, Q.L.; Resources, X.D.; Data curation, Y.Y.; Writing—original draft, Y.L.; Funding acquisition, Y.Z. All authors have read and agreed to the published version of the manuscript.

Funding: This study was supported by National MCF Energy R&D Program (No. 2019YFE03130002).

Institutional Review Board Statement: Not applicable.

Informed Consent Statement: Not applicable.

Data Availability Statement: Data are contained within the article.

Conflicts of Interest: The authors declare no conflict of interest.

References

1. Ongena, J.; Koch, R.; Wolf, R.; Zohm, H. Magnetic-confinement fusion. *Nat. Phys.* **2016**, *12*, 398–410. [CrossRef]
2. Matthews, G. Material migration in divertor tokamaks. *J. Nuclear Mater.* **2005**, *337–339*, 1–9. [CrossRef]

3. Travere, J.; Aumeunier, M.; Joanny, M.; Loarer, T.; Firdaouss, M.; Gauthier, E.; Martin, V.; Moncada, V.; Marot, L.; Chabaud, D.; et al. Imaging Challenges for ITER Plasma-Facing Component Protection. *Fusion Sci. Technol.* **2013**, *64*, 735–740. [CrossRef]
4. Dux, R.; Bobkov, V.; Fedorczak, N.; Iraschko, K.; Kallenbach, A.; Neu, R.; Pütterich, T.; Rohde, V. Tungsten erosion at the ICRH limiters in ASDEX Upgrade. *J. Nucl. Mater.* **2007**, *363*, 112–116. [CrossRef]
5. Rohde, V.; Mertens, V.; Scarabosio, A. Gas balance in ASDEX Upgrade with tungsten first wall. *J. Nucl. Mater.* **2009**, *390*, 474–477. [CrossRef]
6. Tokunaga, K.; Yoshida, N.; Kubota, Y.; Noda, N.; Imamura, Y.; Oku, T.; Kurumada, A.; Sogabe, T.; Kato, T.; Plöchl, L. High heat flux test of actively cooled tungsten-coated carbon divertor mock-ups. *Fusion Eng. Design* **2000**, *49–50*, 371–376. [CrossRef]
7. Matějíček, J.; Koza, Y.; Weinzettl, V. Plasma sprayed tungsten-based coatings and their performance under fusion relevant conditions. *Fusion Eng. Design* **2005**, *75–79*, 395–399. [CrossRef]
8. Neu, R.; Maier, H.; Gauthier, E.; Greuner, H.; Hirai, T.; Hopf, C.; Likonen, J.; Maddaluno, G.; Matthews, G.F.; Mitteau, R.; et al. Investigation of tungsten coatings on graphite and CFC. *Phys. Scr.* **2007**, *T128*, 150–156. [CrossRef]
9. Cho, G.S.; Choe, K.H. Characterization of plasma-sprayed tungsten coating on graphite with intermediate layers. *Surf. Coat. Technol.* **2012**, *209*, 131–136. [CrossRef]
10. Moon, S.Y.; Choi, C.H.; Kim, H.S.; Oh, P.; Hong, B.G.; Kim, S.K.; Lee, D.W. Thick tungsten coating on ferritic-martensitic steel applied with a vacuum plasma spray coating method. *Surf. Coat. Technol.* **2015**, *280*, 225–231. [CrossRef]
11. Han, X.Y.; Liu, X.L.; Wang, D.Z.; Wu, Z.; Duan, B. Copper-based tungsten coating by CVD: Microstructure, thermal shock resistance and interfacial bond force. *Surf. Coat. Technol.* **2021**, *426*, 127778. [CrossRef]
12. Ganne, T.; Crépin, J.; Serror, S.; Zaoui, A. Cracking behaviour of PVD tungsten coatings deposited on steel substrates. *Acta Mater.* **2002**, *50*, 4149–4163. [CrossRef]
13. Gu, Y.K.; Liu, J.; Qu, S.X.; Deng, Y.; Han, X.; Hu, W.; Zhong, C. Electrodeposition of alloys and compounds from high-temperature molten salts. *J. Alloys Compd.* **2017**, *690*, 228–238. [CrossRef]
14. Jiang, F.; Zhang, Y.C.; Li, X.L.; Sun, N.B.; Wang, L.L. Tungsten coating prepared on V-4Cr-4Ti alloy substrate by electrodeposition from molten salt in air atmosphere. *Fusion Eng. Des.* **2014**, *89*, 83–87. [CrossRef]
15. Sun, N.B.; Zhang, Y.C.; Lang, S.T.; Jiang, F.; Wang, L.L. Tungsten coatings electro-deposited on CFC substrates from oxide molten salt. *J. Nucl. Mater.* **2014**, *455*, 450–453. [CrossRef]
16. Qin, W.X.; Xi, X.L.; Zhang, L.W.; Nie, Z.R.; Liu, C.J.; Li, R. The effect of MO_x (M = Zr, Ce, La, Y) additives on the electrochemical preparation of tungsten in eutectic Na_2WO_4-WO_3 melt. *J. Electroanal. Chem.* **2023**, *935*, 117343. [CrossRef]
17. Wang, X.H.; Zhang, L.W.; Xi, X.L.; Nie, Z.R. Electrochemical Dissolution Process of Tungsten Carbide in Low Temperature Molten Salt System. *J. Electrochem. Soc.* **2022**, *169*, 051501. [CrossRef]
18. Nohira, T.; Ide, T.; Meng, X.D.; Norikawa, Y.; Yasuda, K. Electrodeposition of Tungsten from Molten KF-KCl-WO_3 and CsF-CsCl-WO_3. *J. Electrochem. Soc.* **2021**, *168*, 046505. [CrossRef]
19. Qi, Y.F.; Tang, Y.H.; Wang, B.; Zhang, M.; Ren, X.Q.; Li, Y.G.; Ma, Y.T. Characteristics of tungsten coatings deposited by molten salt electro-deposition and thermal fatigue properties of electrodeposited tungsten coatings. *Int. J. Refract. Met. Hard Mater.* **2019**, *81*, 183–188. [CrossRef]